Spallation induced by ultrashort laser pulses at critical tension

F. Vidal, T. W. Johnston, J.-C. Kieffer, and F. Martin
Institut National de la Recherche Scientifique-Énergie, Matériaux, et Télécommunications, C.P. 1020, Varennes (Québec) J3X 1S2, Canada

(Received 14 November 2003; revised manuscript received 18 June 2004; published 29 November 2004)

Spallation, as induced by 50 fs laser pulses at the maximum possible tension (critical tension) in a 25-μm aluminum slab, was investigated by means of a one-dimensional fluid code. In the framework of our defect-free fluid model, spallation takes place through spinodal decomposition, a mechanism that differs from the usual mechanism of growth and coalescence of natural defects. Due to the slowing down of the hydrodynamic processes near critical tension, the spinodal decomposition time scale is about 1 ns. Strain rates of about 10^8 s^{-1} and spall thicknesses of a few microns are obtained, in agreement with recent experiments using short laser pulses. The critical tension in the simulation (12.8 GPa) was somewhat larger than the tension inferred from experiments (8.5 GPa). Because of rapidly decreasing hydrodynamic coupling at higher laser fluences, the required laser spallation threshold fluence as predicted by the code (410 J/cm^2) is far higher than in experiments (25 J/cm^2). This large discrepancy in the spallation threshold fluence values might be due either to differences in the mechanisms through which spallation takes place, or to the specific choice of model for the equation of state.

DOI: 10.1103/PhysRevB.70.184125 PACS number(s): 62.50.+p, 62.20.Mk, 79.20.Ds, 83.85.Pt

I. INTRODUCTION

Spallation is defined as the tension rupture of a material sample due to a rarefaction wave produced by the reflection of a sufficiently strong compression shock wave incident on one of the sample boundaries. In experiments, the incident compression shock waves for spallation have been generated by various means, including among them, projectile impacts, explosions (see Ref. 1 and references therein), proton beams,[2] and laser pulses.[1,3–9] Besides its use for investigations on the mechanical properties of solids in extreme conditions of tension, spallation has found applications in the characterization of the adhesion of thin films.[10,11]

An essential feature of the rarefaction wave dynamics involved in spallation is the existence of a maximum possible supportable tension, or critical tension (generally of the order of 10 GPa[12]), at a value which is characteristic of the defect-free material in question.[5,6] The estimates of the tension achieved in experiments when spallation occurs (termed the spall strength) are usually far below the theoretical critical tension. However, in recent results obtained with short laser pulses of 20–100 ps[7] and 300 ps[8] in thin aluminum foils, the maximum spall strength was estimated to be about 2/3 the theoretical critical tension. (This fraction could be somewhat higher when taking into account temperature effects.[7]) This lower value of spall strength is usually presumed to be due to the fact that the observed spallation actually originates from the natural defects in the material[13] or to defects induced by density fluctuations in a metastable state of matter occurring below critical tension.[5]

When the tension due to the reflection of the rarefaction wave is high enough (even though still well below the theoretical critical tension) and has been exerted over a long enough time, the defects in the solid will, under this high stress, grow, become linked, and finally produce the transverse fractures by which spallation is identified. This may well be the case for long time scales. It seems, however, that with a sufficiently short acoustic driver pulse and a sufficiently low density of defects, the linking of a sufficient number of defects might not have time to occur before the tension dropped again. In that case the material can still be made to fail but necessarily at much higher acoustic driver pulse intensities and at higher tension.[2,6–8] Powerful ultrashort laser pulses thus appear to be the ideal tool to investigate spallation near critical tension.

In this paper we deal with the modeling and understanding of the spallation of matter triggered by ultrashort laser pulses at the theoretical critical tension. As well as being a phenomenon of interest in its own right, the investigation of spallation near critical tension would clearly allow the direct testing, using very short pulses and appropriate materials, of a key feature of models for the equation of state (EOS) in a regime which has been inaccessible until now.

To make contact with the recent spallation experiments of Tamura *et al.*,[9] this paper deals in particular with the modeling of shock waves and spallation induced by 50 fs laser pulses in 25 μm aluminum slabs. Although in those experiments the spall strength[12] was not measured, the strain rate generated was estimated to be in excess of 10^8 s^{-1}. This value is about a factor of ten larger than that obtained using conventional shock production methods.[1] While it is believed that the critical tension could be achieved in some materials at strain rates of 10^8 s^{-1} and higher,[6] this, however, does not seem to be the case for standard thin aluminum foils.[7,8] Nevertheless, the basic features of shock dynamics and spallation at critical tension discussed here, in the specific case of ideal aluminum, will serve as a generic example providing physical insight that can be used for the investigation of more appropriate materials (such as possibly molybdenum[2]).

Since in this paper we focus on matter dynamics near critical tension, the simulations presented here are carried out under the assumption that the defect growth can be neglected below critical tension, which implies that defects are either

initially too rare to play any significant role or that they are "frozen" on the time scale of the fast acoustic pulse regime considered. At this time, one cannot predict just how fast the acoustic driver pulse must be to render defects irrelevant since a general understanding of defect growth mechanisms remains to be developed. One notes that the defect growth models discussed in literature[4,5,13–15] are essentially empirical and might not be appropriate to the fast hydrodynamic regime of interest here.

In the framework of the hydrodynamic model used here, spallation naturally occurs at critical tension because of a common mechanism termed spinodal decomposition,[16] in which inhomogeneous structures develop as a result of symmetry breaking due to thermo/hydro-dynamic instabilities. Spinodal decomposition takes place when the EOS model presents classic van der Waals behavior, with its well-known supercooled vapor and the superheated liquid metastable states. A mechanism involving another variant of spinodal decomposition has been described recently in the modeling of laser ablation using sub-picosecond laser pulses,[17] albeit in a quite different regime near the liquid-vapor critical point. The spallation mechanism, as modeled here, is a direct consequence of the features of the EOS and does not require any additional void growth model. It should be noticed that the more rigorous theoretical approach of molecular dynamics is hardly applicable to simulate the experiments of interest here due to the large number of atoms that such simulations would involve. The investigation performed here using a hydrodynamic model can be considered as a first step in the understanding of matter dynamics near critical tension.

In the next section we presents the hydrodynamic model used in this paper. In Sec. III we describe simulation results for shock propagation and reflection, spallation near critical tension, and the velocity of the rear surface boundary. In Sec. IV we discuss the comparison between simulation results with the experiments. Finally, in Sec. V we summarize and conclude the paper.

II. THE MODEL

For this work we use a one-dimensional Lagrangian code (the same one that was used for work reported earlier[17,18]), with a numerical scheme based on the well-known computer code *MEDUSA*.[19] The code provides a consistent description of the laser-matter interaction, of ablation and of the subsequent propagation of shock waves and rarefaction fans in the solid. The laser energy absorption is calculated by solving the wave equation,[20] in which the complex ac electric permittivity of the matter is defined by means of the Drude model. Thermal and dc electrical conductivities are given by the model of Lee and More.[21] We use distinct temperatures for ions and electrons. Since the pressures involved in our simulations are much higher than the elastic to plastic transition pressure (estimated to be about 0.5 GPa in aluminum), only the plastic regime is considered in this work. The plastic velocity of sound for weak shock waves at solid density is about 5.4 km/s. No energy dissipation mechanism other than the usual artificial viscosity[19] is taken into account in the model.

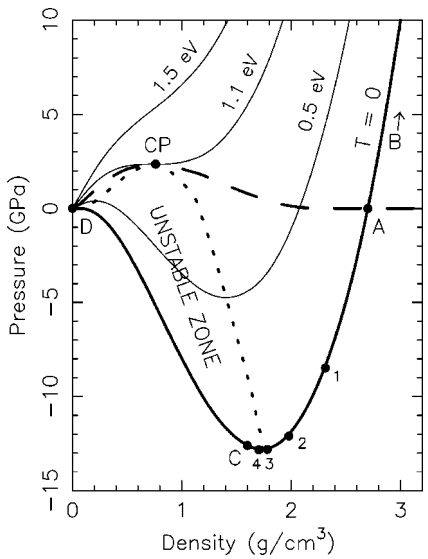

FIG. 1. Phase diagram of aluminum as given by the equation of state QEOS. The isotherms $T=0$, 0.5 eV, 1.1 eV, and 1.5 eV are represented. The "UNSTABLE ZONE" is delimited by the spinodal (dotted line) and the curve $T=0$. Metastable states are between the binodal curve (dashed line), the spinodal curve, and the curve $T=0$. CP is the critical point. Lagrangian cell trajectories of the fractured region are either ABCD or ABCA along the curve $T=0$. Points labeled 1 to 4 correspond to the minimum pressure and density obtained for laser fluences of 25 J/cm^2, 143 J/cm^2, 286 J/cm^2, and 393 J/cm^2, respectively. The critical tension is minus the pressure occurring at the minimum of the curve $T=0$.

The code also includes the quotidian-equation-of-state (QEOS) model that displays a behavior of the van der Waals type, including tension (i.e., negative pressure) at sufficiently low temperatures.[22] The phase diagram of aluminum in the pressure-density plane, as given by QEOS, is shown in Fig. 1 for several isotherms. The phase diagram contains a region, denoted "UNSTABLE ZONE," which is characterized by the relation $(\partial p/\partial \rho)_T < 0$, where p is the pressure, ρ the mass density, and T the temperature. The unstable zone is delimited by the spinodal curve, defined as $(\partial p/\partial \rho)_T = 0$, and by the isotherm $T=0$. In this region, homogeneous matter cannot exist, as "matter cells" tend to evolve randomly toward one of the two branches (high density or low density) of the spinodal curve, separated by the critical point (CP). This matter decomposition process is usually termed spinodal decomposition.[16]

The critical tension given by QEOS is 12.8 GPa and occurs at the density of 1.7 g/cm^3 for $T=0$. These values are about the same as those shown in Ref. 5 (Fig. 7) from a different EOS model for aluminum[23] and in Ref. 2 (Fig. 2) at $T=0$. However, it should be noted that the aluminum EOS presented in Ref. 7 differs significantly from QEOS at higher temperatures, even at 300 K.

III. SIMULATION RESULTS

We have simulated aluminum samples and considered a 50 fs laser pulse with a wavelength of 0.8 μm, an angle of

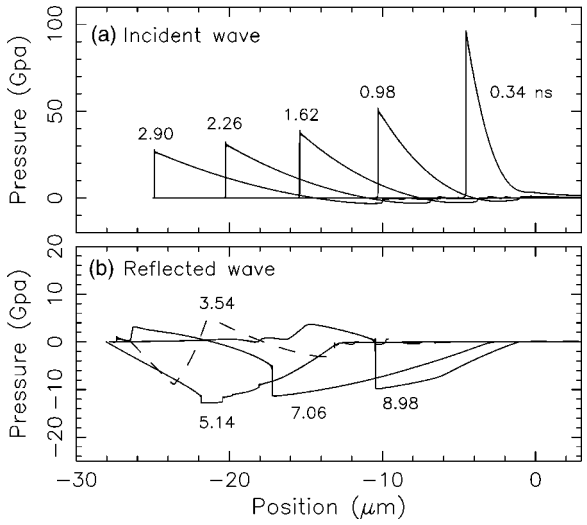

FIG. 2. Pressure of a laser-induced shock wave as a function of position at different times (indicated in nanoseconds) after the laser pulse, for a 25 μm free-standing aluminum foil. The shock is generated on the right by a 50 fs laser pulse with a fluence of 393 J/cm^2.

incidence of 57.5 degrees from a surface normal, and S polarization in order to compare with the spallation experiments presented in Ref. 9. The absorption of ultrashort laser pulses in aluminum has already been modeled successfully in a number of papers.[17,24,25] In the code, the matter is discretized in plane Lagrangian cells of constant surface mass. The surface mass is typically chosen to be 8.1 g/cm^2, which corresponds to a uniform initial spacing of 3 nm between boundaries of the cells in the initial cold solid. An initially finer nonuniform grid has been used near the boundary upon which the laser is incident, in order to calculate accurately the laser energy absorption within the optical skin depth, which is about 10 nm in cold solid aluminum at the wavelength considered.

A. Shock propagation and reflection

Figure 2 shows simulation pressure results for the propagation of the shock wave generated in a 25 μm free-standing aluminum foil in vacuum. The 50 fs laser pulse has been absorbed at the right boundary. In this example, the laser shot yields a greatest tension of 12.8 GPa, for a delay of 5.14 ns after the laser pulse, corresponding to the critical tension predicted by QEOS (see Fig. 1). No spallation occurs in this case for reasons discussed below. The control parameter here is the laser fluence, which for Fig. 2 has a value of 393 J/cm^2. This is just below the spallation threshold fluence, which was determined in our simulations to be 410 J/cm^2. In the simulation, about 42% of the laser energy has been absorbed in aluminum. Of this absorbed energy, most is in the ablated material and little is in the unablated target.

The interaction of the ultrashort laser pulse with the surface triggers a type of *N*-shaped shock wave, or *N*-wave, characteristic of time-limited sources.[26] This *N*-wave propagates to the left, away from the laser-matter interaction region and towards the rear surface, as shown in 2(a). (Note that the lower branch of the *N* is usually more apparent for weaker shocks.) The *N*-wave generates little heat and thus propagates in the solid at near-room temperature. In agreement with the well-known results of asymptotic *N*-wave behavior,[26] the maximum pressure at the *N*-wave shock front decreases asymptotically as $t^{-1/2}$, while the *N*-wave shock itself spreads out as $t^{1/2}$. It should be recalled that the *N*-wave spreading as it progresses is due essentially to the normal convective nonlinearities in the fluid equations and not at all to linear frequency-dependent acoustic dispersion which is not taken into account here. The time evolution of the wave profile can be understood to a large extent by considering that the local wave velocity goes as $(\partial p/\partial \rho)^{1/2}_{T=0}$, where $p(\rho, T=0)$ is shown in Fig. 1.

For free surfaces such as the ones considered here, the effect of reflection in the pressure profile is to reverse the direction of propagation and to change the sign of the pressure. The reflected wave interaction with the incoming wave leads to the rather complicated pressure profile observed at 3.54 ns in Fig. 2(b). Far enough from the reflecting surface, the reflected *N* wave becomes an "anti-*N*-wave" that shrinks as it propagates, as can be observed in the pressure profiles at 7.06 ns and 8.98 ns in Fig. 2(b). As the critical tension is approached (which generally occurs when the tension of the reflected wave is added to that of the incoming *N* wave to give a maximum), the dynamical evolution slows down, as the sound speed is decreasing rapidly, and the wave distorts considerably.

Note, also in Fig. 2(b), that the characteristic spatial region where the tension is within a few percent of the maximum, at a time of 5.14 ns, is something like 2 μm, and the "dwell time" is something like 1 ns. (Clearly, to be more important than spinodal decomposition, a competing spallation mechanism should operate on a scale of a nanosecond or less.) This is determined principally by a combination of the strength of the original *N*-wave impulse and the thickness of the foil, as these parameters have a direct influence on the degree of spreading and weakening of the *N* wave.

B. Spallation at critical tension

When the laser fluence is increased to a value above the threshold value of 410 J/cm^2, our simulations show that the foil breaks up in two main parts. As one should expect, the fracture appears approximately at the place where the critical tension in the rarefaction wave was reached. This distance from the rear surface, often referred to as the spall width, is about 6 μm in Fig. 2(b). Note that no fracture appeared in the near-threshold case considered in Fig. 2 (393 J/cm^2) even though a maximum tension close to 12.8 GPa limit value is indeed obtained. Spinodal decomposition takes time to occur, however, and the duration of the highest tension was apparently not sufficient in the case of Fig. 2.

Figure 3 shows the density profile of the 25-μm aluminum foil for a still greater fluence of 572 J/cm^2, 7.4 ns after the laser pulse. In this case, the *N*-wave shock evolution is very similar to that shown in 2(a), except that now a fracture occurred when the maximum tension was reached. For such

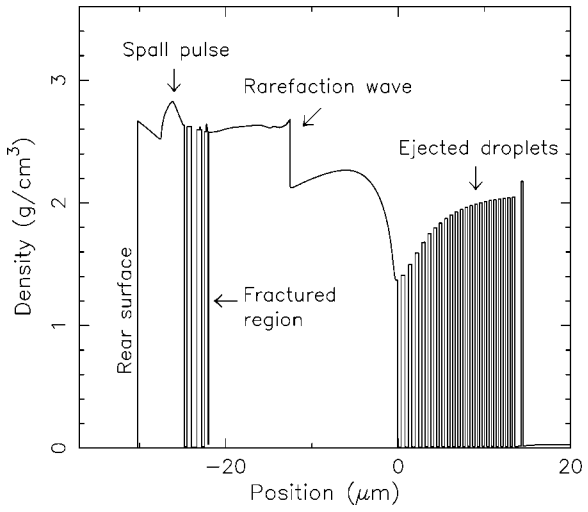

FIG. 3. Density profile of the 25 μm aluminum foil, 7.4 ns after the laser pulse, for a fluence of 572 J/cm^2. The 50 fs laser pulse was absorbed at the right surface.

a fluence well above the threshold, the region between the spalled and unspalled pieces actually contains several very thin foils having typically less than 1 μm width. (Note that such thin layers have been observed in experiments.[9]) For fluences closer to threshold, the initial foil splits in two parts only. Note that the rapid density modulations observed on the far right of Fig. 3, in the laser ablation region, are droplets produced by the critical-point phase separation mechanism discussed in Ref. 17. Since the amount of matter is rigorously constant in the Lagrangian cells of the code, the density minima observed in Fig. 3 are nonzero, essentially being due to the increased size of the corresponding cells. The simulation spall width obtainable from Figs. 2(b) or 3 is about 6 μm. This thickness is similar to the experimentally observed value of 3 μm obtained in Ref. 9.

In Fig. 3 one can also see that, after spallation, a type of *N* wave propagates in each of the two principal portions of the original target. In the spalled region on the left, an *N* wave is traveling toward the left wall. In the right or main foil, an anti-*N*-wave similar to that shown in Fig. 2(b) at 7.06 ns is on its course toward the right boundary.

The process of spallation taking place in the code is illustrated schematically in terms of the trajectories of the Lagrangian matter cells within the density-pressure phase diagram of Fig. 1, by the sequence of steps A to D. The matter cells near the rear surface evolve practically along the isotherm $T=0$ (room temperature would make no difference using QEOS) because little heat is produced by the shock itself and because the heat induced by the laser pulse does not have time to reach the rear boundary through thermal conduction before spallation occurs. Matter cells near the rear surface, initially at rest at the normal solid density of 2.7 g/cm^3 and at zero pressure (A), first undergo an increase in pressure and density (B) due to the compression shock. This is followed by a decrease in pressure and density due to the reflected rarefaction wave. If the tension in the reflected wave is large enough, the relevant matter cells follow the isotherm $T=0$ to enter the unstable zone (C) close to the critical tension, where they undergo forces that expel them outside that thermodynamically unstable zone, either toward the low-density segment of the isotherm (D) or toward the high-density segment (A). The matter cells moving toward the low density part of the isotherm $T=0$ clearly undergo a transition from a high-density phase (of about 1.7 g/cm^3) to the vapor phase. As the density decreases (and the pressure increases) in these vapor cells, more distance separates the high-density foils. When all matter cells have quit the unstable zone, the thin foils so generated are stable in the sense that the number of Lagrangian cells composing them remains constant in time. (Although the details of the fractured region, such as the position of the thin foils and their number, depend on the simulation settings, such as the initial size of the Lagrangian cells and the time step, the threshold fluence for spallation and the spall width depend little on these code parameters provided they are chosen to be sufficiently small. For further details, note that most of the discussion presented in Ref. 17 concerning the droplets induced by the mechanism of critical-point phase separation applies here as well as to the fractured region.)

Figure 1 also shows the absolute minimum pressure and density obtained, at the same position and time, for four fluences chosen below the spallation threshold. Those points, denoted 1 to 4, lie on the curve $T=0$. As the fluence increases, those points get closer to the critical tension. As expected, points 1, 2, and 3 remain outside the unstable zone. However, point 4, which corresponds to the fluence closest to threshold, unexpectedly lies inside the unstable zone. [Note that the corresponding fluence (393 J/cm^2) has been used in Fig. 2.] The explanation for this is likely related to the time taken for spinodal decomposition. For point 4, spinodal decomposition simply did not occur during the short period of time in which the matter remained in the unstable zone. One notes that this particular feature might be difficult to observe if competing spallation mechanisms were taken into account in the framework of a more complete theory.

The spallation process depicted here contains many qualitative resemblances with the model discussed in Ref. 5 in which spallation at a high strain rate is assumed to be induced by fluctuation growth in the superheated liquid (i.e., between the binodal curve and the high-density branch of the spinodal curve in Fig. 1), and thus at tensions smaller than critical. However, in contrast to the latter model, it is clear that in our simulations no phase transitions can take place below the critical tension unless the foil temperature is significant, in which case the matter cells would evolve along higher isotherms and enter the unstable zone at a somewhat lesser tension.

C. Rear surface velocity

Since the rear side of the foil can be located experimentally with laser interferometry,[4,5] it is useful to examine as a diagnostic the velocity of the left hand face in the simulations. The velocity of the rear boundary as a function of time is shown in Fig. 4, for two laser fluences. The first rear velocity plot, for a fluence of 429 J/cm^2 (i.e., above the spallation threshold), is a typical result when spallation does oc-

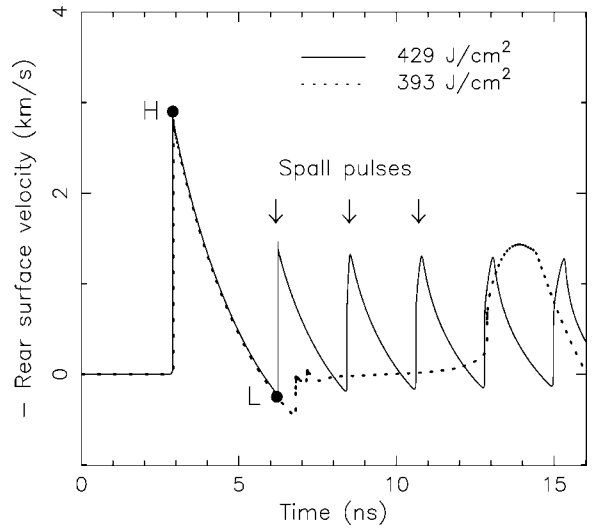

FIG. 4. Minus rear surface velocity as a function of time for two laser fluences (393 J/cm^2 and 429 J/cm^2). Time $t=0$ is defined with respect to the laser pulse. Points H and L correspond to the maximum and the following minimum, respectively, of the first peak in the 429 J/cm^2 case.

cur. The second rear velocity plot, for a fluence of 393 J/cm^2 (below the spallation threshold) is a typical result when spallation does not occur. For the first signal peak, which corresponds to the arrival and reflection of the initial *N* wave, the two cases are the same. However, striking differences are observed after the first pulse between the cases with and without spallation. The later velocity peaks correspond to the arrivals at the rear surface of an *N*-wave shock after each successive round trip. For the no-spallation case, the first round-trip shock arrives about 10 ns after the initial *N*-wave shock. For the spallation case, after an initial delay of about 3 ns, the subsequent inter-peak times (between what are referred to as "spall pulses") are about 2 ns. The explanation for the large change in the inter-pulse times between pulses in the two cases is simple. When spallation takes place, the *N*-wave bouncing is between the boundaries of the thinner spalled foil on the left. When there is no spallation, the wave bounces within the whole unfractured foil. The time between two echoes in a slab of thickness δ is about $2\delta/c_s$ where c_s is the sound velocity. Thus the round trip times are more or less proportional to the thickness of the slab containing the left face, spalled or not as the case may be. It should be noted, however, that for the relatively high laser fluences used here, the shock velocities can significantly exceed the plastic sound velocity in aluminum in normal conditions. Spall pulses have indeed been observed in experiments[4,5] although the spall pulses are not as clear and regular as the ones shown in Fig. 4.

As just noted for the spallation case (429 J/cm^2), while the sequence of round-trip spall pulses have an interval time of 2 ns, the time between the arrival of the first and the second wave fronts is instead 3 ns, or 1 ns more than the others. Rather than being due to an increased travel time, this one time 1 ns delay reflects the significant time required for the actual formation of the spall boundary and the subsequent emission towards the rear surface of the *N*-wave echo. As the tension approaches the critical value, the local wave velocity decreases significantly and the wave in effect more or less stagnates while spallation takes place, being subsequently re-emitted towards the rear boundary in the spalled slab.

Rear-face velocity results allow an immediate estimation of the strain rate. The strain rate obtained in our simulations can be estimated from Fig. 4 by means of the expression used elsewhere:[5]

$$\dot{\epsilon} = \left| \frac{u_H - u_L}{t_H - t_L} \right| \frac{1}{2c_s}, \tag{1}$$

where u_H and u_L are defined, respectively, as the first maximum of the rear surface velocity and the following first minimum, while t_H and t_L are the corresponding times. Applying Eq. (1) to the velocities shown in Fig. 4, for 429 J/cm^2, one finds 8×10^7 s^{-1} (using the plastic sound velocity in aluminum in normal conditions, $c_s=5.4$ km/s) which is close to the value of the order of 10^8 s^{-1} inferred from experiments in aluminum using short laser pulses.[9]

IV. COMPARISON WITH EXPERIMENTS

There is a general remark to be made concerning an important disagreement between the fluences required for spallation in simulations and in experiments. In Fig. 1 we have represented a particular point, denoted by 1, which corresponds to the absolute minimum pressure and density found (at the same position and time) for the laser fluence of 25 J/cm^2 used in the experiments of Tamura *et al.* One observes that the maximum tension achieved is about 8.5 GPa, which represents 2/3 of the critical tension of 12.8 GPa given by QEOS. While these two values differ significantly, their ratio is still of the order of 1. However, the ratio of the fluences required to obtain 8.5 GPa (i.e., 25 J/cm^2) is only 6% of the simulation fluence required to reach the QEOS value of 12.8 GPa (410 J/cm^2 for S polarization), a very strong disagreement indeed. Since the ratio of the fluences (about 16:1) is roughly ten times higher than the ratio of the critical tensions (12.8 GPa to 8.5 GPa, for a ratio of 3:2), one can conclude that, while laser fluence is a useful control parameter for experiment and simulation alike, the ratio between fluences does not allow a useful estimate of shock amplitudes. This is largely because, as the fluence is increased, the conversion of laser energy into hydrodynamic energy launched into the cold target decreases dramatically as more and more of the absorbed energy goes into the ablated material. (Less than 10% of the incident laser energy is converted into kinetic energy in the unablated target.) We note that a somewhat smaller threshold of 260 J/cm^2, calculated using P polarization, was obtained, taking into account resonant absorption only. While noticeably lower than for S polarization, this threshold is still much higher than in the experiments.

Returning to the spallation threshold tension, several explanations for this disagreement between the model and the experiments can be put forward. Under the assumption that spallation actually occurs at critical tension in the experiments, a first explanation would be that the EOS model used

in this paper (QEOS) considerably overestimates the aluminum critical tension. If the critical tension was much smaller than expected from QEOS, then the theoretical spallation threshold fluence would be lower and thus in better agreement with experiments. A second explanation is that spallation observed in the experiments does not occur at critical tension and can still be due to the growth of natural defects, even though the laser pulse is very short indeed and even though strain rates are higher than 10^8 s^{-1}. As to the defect levels in the experiments of Tamura *et al.*, no particular precautions were mentioned as being taken to use bulk aluminum so as to be as defect-free as possible. Thus one cannot say anything about the density of defects of the aluminum used. If the aluminum samples used in the experiments were to contain a sufficient density of natural defects, then those defects might be enough to trigger spallation at a tension $2/3$ of the critical value, and thus at laser fluences far smaller than predicted by our model. A third explanation, already mentioned in the Introduction, is that proposed in Ref. 5. This explanation does not involve defects and yet accounts for a somewhat lower critical tension for spallation. In that picture the spallation at a high strain rate would be induced by fluctuation growth in the metastable superheated liquid, at tensions smaller than critical and well before the unstable region is reached.

It is interesting to note that this value of 8.5 GPa obtained here at 25 J/cm^2, in connection with the experiments of Tamura *et al.*, nearly coincides with the spall strength of 9 GPa inferred in Refs. 7 and 8, where 10 ps–300 ps laser pulses were used. This result could be explained by the fact that, as one sees from Fig. 2(a), the *N*-wave generated by the 50 fs laser pulse spreads and weakens considerably as it propagates, as a consequence of the usual nonlinear hydrodynamic effects. These effects become less significant as the shock weakens. Therefore, after having propagated over 25 μm, the features of the *N* waves generated by ultrashort laser pulses will be comparable to those generated by much longer pulses.

As a final comment, we note that, although the strain rate obtained from the simulations is about 10^8 s^{-1}, as inferred indirectly in the experiments of Tamura *et al.*, the spall width is two times larger in the simulations (6 μm) than in experiments (3 μm). This higher value might be due to the higher fluence required to achieve spallation in the simulations, since the spreading of the *N* wave is faster at a higher fluence due to stronger nonlinear hydrodynamic effects.

V. SUMMARY AND CONCLUSION

In this paper we have presented a theoretical investigation of spallation induced by powerful 50 fs laser pulses in aluminum slab samples, with results chosen to illustrate the behavior just above and just below the spallation threshold near critical tension. In the framework of the fluid model presented here, the spallation process takes place through spinodal decomposition, a mechanism which involves a spontaneous transition of some high-density Lagrangian cells into a gaseous phase. This is the only spallation mechanism that has been taken into account in our calculations.

From the simulation results for defect-free aluminum, here we emphasize two useful points in order to understand the generic hydrodynamics related to spallation at critical tension. The first point is one of basic hydrodynamic behavior: the *N* waves generated by means of ultrashort laser pulses at high fluence spread and weaken rapidly as a function of the distance as a consequence of nonlinear hydrodynamic effects. Therefore, in order to investigate spallation at higher tensions, ultrashort laser pulses must be used in combination with very thin foils (a few microns) in order to retain all the specific features of strength and shortness of the *N* waves triggered by this means. The second point we stress is that the physics in the pre-spall becomes much slower as the sound velocity tends to zero. In a phrase, spallation at critical tension is a slow process. We propose that this feature of the spallation process observed in the simulations is likely to be generic, i.e., one whose general behavior depends weakly on the subsequent spallation mechanism. The nanosecond delay that is required to achieve spinodal decomposition at the critical tension suggests that other spallation mechanisms, like the growth of natural defects or phase transitions, could equally well have enough time to take place. This "softening" of matter could well be a generic feature of matter at very high tension that could be observed using fast optical techniques (for instance by measuring the delay between the main pulse and the subsequent spall pulses).

A comparison of the simulations presented here with the pertinent experimental results of Tamura *et al.* allows two immediate conclusions. The first conclusion is that the tension of 8.5 GPa inferred from our code, using the same laser parameters as in the experiments, is about $2/3$ of the critical tension predicted by the EOS model we used (QEOS). As remarked above, this discrepancy could be due to the imperfection of the critical tension predicted by the EOS considered or to the influence of the usual spallation mechanisms, which may still dominate the process. The second conclusion is that there is a very much larger ratio between the fluence used in the experiments to achieve spallation (25 J/cm^2 for a tension of 8.5 GPa) and the fluence required by the model (410 J/cm^2 for a tension of 12.8 GPa) to attain the predicted critical tension. We believe that this is merely a reflection of the decreasing fraction of the laser energy available as a hydrodynamic driver as the fluence is increased. The important practical conclusion is that, while the laser fluence is a useful experimental control parameter, it is not a simple measure of the energy in the acoustic driver which is to produce spallation. Shock waves are more appropriately characterized by inferring the pressure and strain rate at the rear boundary from measurements of the rear surface velocity as a function of time.

Finally, let us point out that the general dynamical behavior of the material with a realistic level of defects might well resemble, at least qualitatively, that of the present model, but scaled down to the lower stresses at which the defective material will fail. It would be a considerable challenge to develop a general dynamical model of an equation of statecombined with an irreversible process of defect growth, with a stress threshold, and a stress-dependent ensemble growth rate, but it is one likely worth the attempt. Such a detailed

model could be used only to describe the behavior of matter near critical tension while most of the shock evolution could be calculated using a faster model such as the one discussed in this paper.

ACKNOWLEDGMENTS

This work was financed partly by the National Science and Engineering Research Council of Canada (NSERC).

[1] S. Eliezer, I. Gilath, and T. Bar-Noy, J. Appl. Phys. **67**, 715 (1990).
[2] G. I. Kanel, S. V. Razorenov, A. V. Utkin, V. E. Fortov, K. Baumung, H. U. Karow, X. Rusch, and V. Licht, J. Appl. Phys. **74**, 7162 (1993).
[3] F. Cottet and M. Boustie, J. Appl. Phys. **66**, 4067 (1989).
[4] L. Tollier, R. Fabbro, and E. Bartnicki, J. Appl. Phys. **83**, 1224 (1998); L. Tollier and R. Fabbro, *ibid.* **83**, 1231 (1998).
[5] E. Dekel, S. Eliezer, Z. Henis, E. Moshe, A. Ludmirsky, and I. B. Goldberg, J. Appl. Phys. **84**, 4851 (1998).
[6] E. Moshe, S. Eliezer, E. Dekel, Z. Henis, A. Ludmirsky, I. B. Goldberg, and D. Eliezer, J. Appl. Phys. **86**, 4242 (1999).
[7] E. Moshe, S. Eliezer, Z. Henis, M. Werdiger, E. Dekel, Y. Horovitz, S. Maman, I. D. Goldberg, and D. Eliezer, Appl. Phys. Lett. **76**, 1555 (2000).
[8] W. H. Zhu, M. Yoshida, H. Tamura, K. Kondo, and S. Tanimura, J. Mater. Sci. Lett. **20**, 961 (2001).
[9] H. Tamura, T. Kohama, K. Kondo, and M. Yoshida, J. Appl. Phys. **89**, 3520 (2001).
[10] M. Boustie, E. Auroux, J. P. Romain, and M. Jeandin, J. Phys.: Condens. Matter **14**, 10839 (2002).
[11] M. Zhou, Y. K. Zhang, and L. Cai, Appl. Phys. A: Mater. Sci. Process. **74**, 475 (2002).
[12] D. E. Grady, J. Mech. Phys. Solids **36**, 353 (1988).
[13] V. E. Fortov, V. V. Kostin, and S. Eliezer, J. Appl. Phys. **70**, 4524 (1991).
[14] D. Chen, S. Di-Hassani, M. Sarumi, and X. Jin, Int. J. Impact Eng. **19**, 107 (1997).
[15] F. Tuler and B. Butcher, Int. J. Fract. Mech. **4** 431 (1968).
[16] V. P. Skripov and V. A. Skripov, Sov. Phys. Usp. **22**, 389 (1979).
[17] F. Vidal, T. W. Johnston, S. Laville, O. Barthélemy, M. Chaker, B. Le Drogoff, J. Margot, and M. Sabsabi, Phys. Rev. Lett. **86**, 2573 (2001).
[18] S. Laville, F. Vidal, T. W. Johnston, O. Barthélemy, M. Chaker, B. Le Drogoff, J. Margot, and M. Sabsabi, Phys. Rev. E **66**, 066415 (2002).
[19] J. P. Christiansen, D. E. T. F. Ashby, and K. V. Roberts, Comput. Phys. Commun. **7**, 271 (1974).
[20] J.-C. Kieffer, J.-P. Matte, S. Bélair, M. Chaker, P. Audebert, H. Pépin, P. Maine, D. Strickland, P. Bado, and G. Mourou, IEEE J. Quantum Electron. **25**, 2640 (1989).
[21] Y. T. Lee and R. M. More, Phys. Fluids **27**, 1273 (1984).
[22] R. M. More, K. H. Warren, D. A. Young, and G. B. Zimmerman, Phys. Fluids **31**, 3059 (1988).
[23] A. V. Bushman, G. I. Kanel, A. L. Ni, and V. E. Fortov, *Intense Dynamic Loading of Condensed Matter* (Taylor and Francis, London, 1993), Chaps. 5, 8.
[24] A. Ng, P. Celliers, A. Forsman, R. M. More, Y. T. Lee, F. Perrot, M. W. C. Dharma-wardana, and G. A. Rinker, Phys. Rev. Lett. **75**, 252 (1995).
[25] K. Eidmann, J. Meyer-ter-Vehn, T. Schlegel, and S. Hüller, Phys. Rev. E **62**, 1202 (2000).
[26] R. Courant and K. O. Friedrichs, *Supersonic Flow and Shock Waves* (Wiley, New York, 1948), Vol. I, p. 164.